


Combined Anti-Angiogenic and Anti-Inflammatory Nanoformulation for Effective Treatment of Ocular Vascular Diseases

Jianguo Sun^{1,*}, Huiling Nie^{2,*}, Panpan Pan^{3,*}, Qin Jiang^{2,*}, Chang Liu¹, Min Wang¹, Yonghui Deng^{3,4}, Biao Yan¹ 

¹Eye Institute and Department of Ophthalmology, Eye & ENT Hospital, State Key Laboratory of Medical Neurobiology, Fudan University, Shanghai, People's Republic of China; ²The Affiliated Eye Hospital and The Fourth School of Clinical Medicine, Nanjing Medical University, Nanjing, People's Republic of China; ³Department of Chemistry, Fudan University, Shanghai, People's Republic of China; ⁴Department of Gastroenterology and Hepatology, Zhongshan Hospital, Institute of Biomedical Sciences, Fudan University, Shanghai, People's Republic of China

*These authors contributed equally to this work

Correspondence: Yonghui Deng; Biao Yan, Email yhdeng@fudan.edu.cn; biao.yan@fdeent.org

Background: Ocular vascular diseases are the major causes of visual impairment, which are characterized by retinal vascular dysfunction and robust inflammatory responses. Traditional anti-angiogenic or anti-inflammatory drugs still have limitations due to the short-acting effects. To improve the anti-angiogenic or anti-inflammatory efficiency, a dual-drug nanocomposite formulation was proposed for combined anti-angiogenic and anti-inflammatory treatment of ocular vascular diseases.

Methods: CBC-MCC@hMSN(SM) complex nanoformulation was prepared by integrating conbercept (CBC, an anti-angiogenic drug) and MCC950 (MCC, an inhibitor of inflammation) into the surface-modified hollow mesoporous silica nanoparticles (hMSN(SM)). CBC-MCC@hMSN(SM) complex nanoformulation was then characterized by Fourier transform infrared spectroscopy, transmission electron microscopy, zeta potentials, and nitrogen adsorption-desorption measurement. CBC and MCC release profile, cytotoxicity, tissue toxicity, anti-angiogenic effects, and anti-inflammatory effects of CBC-MCC@hMSN(SM) were estimated using the in vitro and in vivo experiments.

Results: CBC-MCC@hMSN(SM) complex had no obvious cytotoxicity and tissue toxicity and did not cause a detectable ocular inflammatory responses. CBC-MCC@hMSN(SM) complex was more effective than free CBC or MCC in suppressing endothelial angiogenic effects and inflammatory responses in vitro. A single intraocular injection of CBC-MCC@hMSN(SM) complex potently suppressed diabetes-induced retinal vascular dysfunction, choroidal neovascularization, and inflammatory responses for up to 6 months.

Conclusion: Combined CBC and MCC nanoformulation provides a promising strategy for sustained suppression of pathological angiogenesis and inflammatory responses to improve the treatment outcomes of ocular vascular diseases.

Keywords: combined nanocomposite formulation, mesoporous silica nanoparticle, anti-angiogenesis, anti-inflammation, ocular vascular disease

Introduction

Pathological angiogenesis is recognized as the major cause of vision impairment and eventual blindness in the world, including corneal neovascularization, choroidal neovascularization (CNV), and diabetic retinopathy (DR).¹ Pathological factors, such as hyperglycemia, oxidative stress, and hypoxia, can disrupt the normal vasculature and cause vascular dysfunction.^{2,3} Vascular dysfunction further leads to the activation of inflammatory cells, contributing to the inflammatory cell filtration and inflammation cascades.⁴ Angiogenesis and inflammation is interconnected with each other and pro-inflammatory factors usually have pro-angiogenic effects and vice versa.⁵ Pathological angiogenesis and inflammatory responses have been involved in the pathogenesis of ocular vascular diseases.⁶

Currently, drug treatments for pathological angiogenesis are mainly dependent on the inhibitors targeting vascular endothelial growth factor (VEGF) signaling, such as bevacizumab, lucentis, aflibercept, and conbercept (CBC). These drugs are often short-acting and required for repetitive intraocular injection to maintain the therapeutic efficiency.⁷ However, repetitive injections of anti-VEGF drugs are very expensive and have several side effects on normal vessels, which may lower the patient compliance and cause the poor adherence to anti-VEGF treatment.⁸ Anti-inflammatory treatment is achieved by the application of corticosteroids, such as prednisolone and dexamethasone, which are hourly administered by the topical eye drops to inhibit ocular inflammation.⁹ However, it is often followed by the gradual decrease of the medication and cessation of therapy due to the rapid elimination and short-acting time.¹⁰ Given the angiogenesis-inflammation interconnection and short-acting effects of current anti-angiogenic/anti-inflammatory drugs, it is better to use drug combinations for combined anti-angiogenic and anti-inflammatory treatment and develop a novel drug delivery system to improve the drug bioavailability and the duration of drug action.^{11,12}

Conbercept (CBC) is a recombinant fusion protein, which has been approved as a decoy receptor for VEGF and placental growth factor for treating ocular vascular diseases, such as neovascular age-related macular degeneration, diabetic macular edema, and retinopathy of prematurity (ROP).^{13–15} MCC950 (MCC) is a specific small molecule inhibitor of the canonical and non-canonical activation of NLRP3 inflammasome, which shows the great potentials for treating inflammatory diseases.¹⁶ CBC (143 kDa) is a big molecule drug, while MCC (426 Da) is a small molecule drug. Small molecule drugs are easily consumed or metabolized away by ocular circulation and have short short-acting time.¹⁷ Thus, it is necessary to design a novel drug delivery system for sustained release of CBC and MCC and enhance their bioavailability and duration of drug action.

Several nanocarriers have been used for the delivery of ocular drugs.^{18,19} Among these nanocarriers, mesoporous silica nanoparticles (MSNs) have attracted great attentions due to the distinctive properties, such as high specific surface areas, large pore volumes, well-defined pore structures, and tunable pore sizes,^{20–22} especially the good biodegradability and reliable biocompatibility.^{23,24} MSNs have been used to deliver the small molecular drugs (nitric oxide donor, pilocarpine) to treat ocular hypertension and the macromolecular drug (bevacizumab) to improve the anti-angiogenic efficiency.^{25–27} In this study, we designed a novel MSN nanoparticle with the rambutan-like rough surfaces and the well-interconnected nanopores for the co-delivery of CBC (a macromolecule drug) and MCC (a small molecule drug). We also determined the anti-angiogenic and anti-inflammatory efficacy of CBC-MCC@hMSN(SM) complex nanoformulation in the treatment of ocular vascular diseases.

Materials and Methods

Synthesis of hMSN(SM) Nanocarrier

hMSNs were synthesized via a co-condensation process of resorcinol, formaldehyde, and silica species.²⁸ Briefly, resorcinol (0.15 g) and formaldehyde (37%, 0.21 mL) were added to the mixture composed of ammonia aqueous solution (28%, 3.0 mL), deionized water (10 mL), and anhydrous ethanol (70 mL). The mixture was vigorously stirred for 6 h at room temperature. After the addition of different volume of TEOS (0.7, 1.2, or 1.6 mL), the mixture was stirred for 8 min before the addition of resorcinol (0.40 g) and formaldehyde (37%, 0.56 mL). The mixture was then stirred for 2 h at room temperature. The synthesized products were collected by centrifugation, ethanol washing, and dried at 50 °C. Finally, hMSNs were harvested after the calcination at 550 °C for 5 h in the air.

Surface functionalization of hMSNs consisted of -NH₂-modification and PEG-modification.²⁵ Briefly, 30 mg of hMSNs was dispersed in 25 mL of anhydrous ethanol plus 50 µL of APTES. Then, the mixture was stirred at 70 °C for 3 h. The products were collected by centrifugation and washed with anhydrous alcohol. The products were dried at 110 °C for 3 h, followed by vacuum dry for 24 h to obtain NH₂-modified hMSNs (hMSN-NH₂). Then, hMSN-NH₂ products were dispersed in 10 mL of MES buffer. Then, another 5 mL of MES buffer with 5 mg of mPEG-NHS was added. The mixture was stirred at room temperature for 3 h. PEG-modified hMSNs (hMSN-NH₂-PEG) were collected by centrifugation and washed with deionized water to remove the unreacted mPEG-NHS. hMSN-NH₂-PEG products were lyophilized to obtain the functionally modified hMSNs, abbreviated as hMSN(SM) (SM: surface-modified). hMSN(SM) was sterilized by UV irradiation for 20 min and used for nanocomposite formulations.

Preparation and Characterization of CBC-MCC@hMSN(SM) Complex

Nanoformulation

MCC and CBC were in sequence loaded into hMSN(SM) via the nanocasting strategy to obtain MCC@hMSN(SM), CBC@hMSN(SM), or CBC-MCC@hMSN(SM) complex.²⁹ Briefly, MCC and hMSN(SM) were dissolved in deionized water. After stirring at 300 rpm for 2 h, MCC@hMSN(SM) was collected via centrifugation at 12,000 rpm, washed 3 times by deionized water, and then dispersed in deionized water again. CBC was mixed with the above dispersion. After stirring at 300 rpm for 6 h at 4 °C, the samples were collected by centrifugation at 12,000 rpm and washed away CBC. These samples were dispersed in normal saline again, collected by freeze drying, and stored under -20 °C. At the washing step, the supernatants were collected and the amounts of MCC and CBC in the supernatant were determined by LC-MS/MS and ELISA assays, respectively. Encapsulation efficiency and drug loading efficiency were calculated as shown below.²⁵

Encapsulation Efficiency (%) = Amount of encapsulated drug/Amount of total drug × 100%

Loading Efficiency (%) = Amount of encapsulated drug/Total weight of hMSN(SM) × 100%

Amount of encapsulated drug = Total drug – Free drug in the supernatant.

The morphology, particle size, and particle size distribution of hMSN and hMSN(SM) nanocarriers were characterized by TEM (JEOL 2011 Microscope). The zeta potentials of hMSN and hMSN(SM) nanocarriers were measured in deionized water on Zetasizer Malvern Instrument (Malvern). Nitrogen adsorption-desorption measurements were conducted on a Micrometrics Tristar 3000 analyzer at 77 K. The specific surface areas were calculated using the Brunauer-Emmett-Teller (BET) model in the relative pressure (P/P_0) ranging from 0.04 to 0.1. The pore size distribution and pore volume were calculated using the Barrett-Joyner-Halenda (BJH) model. Total pore volumes (V_t) were calculated based on the adsorbed N₂ amount at the P/P_0 of 0.995. The surface-modification of hMSNs by -NH₂ and -PEG groups were characterized using the FTIR on a Nicolet 6700 spectrometer (Thermo fisher) via KBr disc at a resolution of 4 cm⁻¹ in the frequency interval of 500–4000 cm⁻¹. The surface roughness was defined as D_p/D_a , in which D_a represented the diameter calculated from hMSN shadow area, while D_p was the diameter calculated from hMSN shadow perimeter. hMSN shadow area and hMSN shadow perimeter were obtained by measuring hMSN nanoparticles based on TEM images using Image J software.

In vitro Release Study of CBC and MCC from CBC-MCC@hMSN(SM) Complex Formulation

To determine the release profiles of CBC and MCC from CBC-MCC@hMSN(SM) complex formulation in vitro, the freshly prepared MCC@hMSN(SM) (1 mg MCC), CBC@hMSN(SM) (2 mg CBC), or CBC-MCC@hMSN(SM) (2 mg CBC and 1 mg MCC) complex were filled into the dialysis bags (cut-off MW 300 kDa). The dialysis bags with the samples were distributed in 20 mL of PBS and placed in the incubator water bath at 37 °C. At the specific time intervals (3, 6, 9, 18, 26 h, and 2, 4, 6, 10, 16, and 28 d), 3 mL of leaching liquor was withdrawn and 3 mL of fresh PBS was added to the solution to keep the sink condition. The withdrawn mediums were stored at -20 °C and concentrated by freeze drying and dissolving. The concentration of MCC was detected by LC-MS/MS and the concentration of CBC was detected by ELISA assays. The details of LC-MS/MS and ELISA assays were shown in the [Supplementary Information](#). The cumulative release curves of MCC@hMSN(SM), CBC@hMSN(SM) and CBC-MCC@hMSN(SM) complex were plotted against time.

Detection of Cytotoxicity by MTT Assay

Human retinal vascular endothelial cells (HRVECs) were purchased from Cell Systems Corporation (UK). Rhesus macaque choroid-retinal endothelial cell line (RF/6A cell) was purchased from the American Tissue Culture Collection (USA). They were cultured in DMEM/F12 (1:1) medium supplemented with 10% of FBS in 5% CO₂ at 37°C. HRVECs (n = 4) or RF/6A cells (n = 4) were incubated with different concentrations (0.1, 1, 10, 100 and 1000 µg/mL) of hMSN(SM) nanocarrier for the indicated time points. These cells were washed with PBS for 3 times and

incubated with MTT (0.5 mg/mL) for 3 h. Dimethyl sulfoxide solution was used to dissolve formazan crystals. MTT absorbance was determined by a microplate reader (FliterMax F5, Molecular Devices, USA).³⁰

Cell Proliferation Assay

Cell proliferation was determined by Ki67 staining.²⁵ HRVECs were cultured in 24-well plates at a density of 5×10^4 cells per well, and then treated with VEGF without or with hMSN(SM), CBC, MCC, CBC@hMSN(SM), MCC@hMSN(SM), or CBC-MCC@hMSN(SM) complex for the indicated time points. After the required treatment, they were fixed in 4% formaldehyde for 15 min, blocked with 5% BSA for 30 min, incubated with Ki67 antibody (1:200, Abcam) at 4 °C overnight, and incubated with the fluorescent secondary antibody (1:500, Abcam) for 3 h at room temperature. Finally, they were stained with DAPI (1:1500, Abcam) to show nuclei and photographed under a fluorescence microscope (IX-73, Olympus, Japan).

Cell Migration Assay

Cell migration was determined using the transwell chamber (24-well, 8.0- μ m pore membranes, Corning).³¹ Briefly, HRVECs (5×10^4 per well) were seeded onto the upper chamber in 100 μ L of serum-free medium. About 500 μ L of complete medium was added to the lower chamber as the chemoattractant. After the required treatment, HRVECs were cultured for 12 h at 37 °C. The migrated cells were fixed with methyl alcohol for 15 min and stained with 0.5% crystal violet for 30 min. These non-migrated cells were removed using a cotton swab. The number of migrated cells was counted under a microscope (IX-73, Olympus, Japan).

Tube Formation Assay

Tube formation ability was determined by incubating HRVECs with different complex nanoformulations.²⁵ After the required treatments, HRVECs were digested by 3% trypsin and re-suspended in DMEM medium. Each well of 24-well plate was coated with 50 μ L of the growth factor-reduced Matrigel followed by the incubation for 30 min at 37 °C to allow gelation. HRVECs were seeded onto the Matrigel (2×10^5 cells per well). The tube-like networks were observed under a microscope (IX-73, Olympus, Japan).

LPS-Induced Inflammatory Response in HRVECs

Lipopolysaccharide (LPS) was used to induce the inflammatory response.³² HRVECs were seeded onto a 24-well plate and incubated for 24 h to allow cell attachment. Then, they were stimulated with LPS (100 ng/mL). After the required treatments, the expression levels of ICAM-1, MCP-1, VEGF, and IL-6 were detected by qRT-PCRs and ELISA assays.

Animal Experiment

All animal experiments adhered to the guidelines of ARVO Statement for the Use of Animals in Ophthalmic and Vision Research and were approved by the Animal Care and Use Committee of the authors' institute. C57BL/6J mice (6–8 weeks old, male) were obtained from Qinglongshan Experimental Animal Center (Nanjing, China) and kept under a pathogen-free condition with alternating 12/12 h light-dark cycle, ensuring free access to standard normal diet and water.

Estimation the Biosafety of hMSN(SM) Nanocarrier in vivo

The biosafety of hMSN(SM) nanocarrier was determined by intravitreal injections of 1 μ L of different concentrations of hMSN(SM) (1, 10, and 100 μ g/mL) nanocarrier into the eyes of C57BL/6J mice. Retinal histological structures and retinal apoptosis were detected by H&E staining and TUNEL staining. The expression changes of ICAM-1, MCP-1, VEGF, and IL-6 levels were detected by ELISA assays.³³

In vivo Release Study of CBC and MCC from CBC-MCC@hMSN(SM) Complex Formulation

In vivo release of MCC and CBC from CBC-MCC@hMSN(SM) complex was studied through an intravitreal injection of 1 μ L of CBC-MCC@hMSN(SM) (CBC: 10 mg/mL, MCC: 5 mg/mL) or an equivalent amount of free MCC or CBC into the eyes of C57BL/6J mice. At day 0 and day 30 after injection, C57BL/6J mice were executed and the retinas were dissected out from the enucleated eyes. The remaining MCC amount in the retina was detected by LC-MS/MS method. The remaining CBC amount in the retina was detected by ELISA assays.^{34,35}

Laser-Induced Experimental CNV Model

The experimental CNV model was induced by laser photocoagulation with the rupture of Bruch's membrane.³⁶ The pupils of C57BL/6J mice were dilated using the tropicamide phenylephrine eye drops (Santen, China). Laser photocoagulation (647 nm; 50 mm spot size; 0.05 s duration; 250 mW) was conducted to burn the retinas at the 3, 6, 9, and 12 o'clock positions. The laser spots were created with ~2–3 disk diameters from optic nerve head. The sign of Bruch's membrane rupture was the formation of bubbling at the site of laser photocoagulation. After Bruch's membrane rupture and treated with hMSN(SM), MCC, MCC@hMSN(SM), CBC, CBC@hMSN(SM), or CBC-MCC@hMSN(SM) complex, Isolectin-B4 staining was conducted to detect neovascular areas of RPE/choroid flat mounts.

Streptozocin-Induced Diabetic Model

Diabetic model was induced in C57BL/6J mice (6–8 weeks old, male) by an intraperitoneal injection of streptozocin (STZ, 75 mg/kg).³¹ The control group received an intraperitoneal injection of vehicle (citrate buffer). The blood glucose level was measured at 48 h after STZ injection and monitored weekly thereafter. Diabetes mellitus was confirmed by the fasting blood glucose level more than 250 mg/dL.

Evans Blue Staining

Retinal vessel permeability was determined using Evans blue assay.³⁷ Briefly, Evans blue (30 mg/kg) was injected through a jugular vein catheter after deep anesthesia. Two hours later, about 0.1 mL of blood sample was collected. The eyes were enucleated and the retinas were dissected out. Evans blue was extracted from the retinas and then incubated in 0.3 mL of formamide overnight at 70 °C. The blood samples and extraction solutions were collected by centrifugal separation at 12,000 g for 15 min at 4 °C. The sample solutions were filtered through a 30,000-molecular weight filter and Evans blue signaling was detected at 620 nm and 720 nm. The concentration of Evans blue in the supernatants was calculated from the standard curve of Evans blue and normalized to dry retinal weight and time-averaged concentration of Evans blue in the plasma.

PAS/Hematoxylin Staining

PAS (Periodic Acid-Schiff)/hematoxylin staining was used to detect the structure changes of retinal vessels.³⁷ The retinas were fixed in 4% paraformaldehyde, dissected out from the eyecups, and digested in 3% trypsin for 2–3 h at 37 °C. Retinal vessels were separated from other retinal neuronal cells by gentle shaking under a dissection microscope. The vessels were mounted on a slide, allowed to dry, and stained with PAS/hematoxylin (Glycogen PAS Stain Kit). After staining and washing in water, retinal vessels were dehydrated and mounted using the Permunt mounting media (Sigma, St. Louis, MO, USA). Retinal vasculature was observed under a microscope (DP80, Olympus, Japan). Acellular capillaries were counted from the images for each retina and expressed as the number of acellular vessels per mm².

Statistics

All measurements were taken from the distinct samples (n) and data were presented as mean \pm SD. Statistical significance was determined by Student's *t*-test for two groups and one-way ANOVA followed by the post hoc Bonferroni test for multiple groups if the data were normally and equally distributed. The nonparametric Mann–Whitney *U*-test or Kruskal–Wallis test followed by the post hoc Bonferroni test was used to compare abnormal

distribution data. The value of $P < 0.05$ was considered statistically significant. OriginPro 9.0 (OriginLab Corporation, USA) and GraphPad Prism 8 (GraphPad, San Diego, CA, USA) were used for statistical analysis.

Results

Characterization of CBC-MCC@hMSN(SM) Complex Formulation

The hMSNs with the rambutan-like rough surfaces and hollow cavities interconnected with a plenty of mesoporous were synthesized via the sol-gel chemistry technique. hMSNs had discrete spheres with the average diameter of 250 ± 10 nm. The magnified images and the outlines of hMSNs showed that they had the rambutan-like rough surfaces (Figure S1A and Figure 1A). The surface roughness of hMSNs (D_p/D_a) gradually increased from 2.1 ± 0.3 to 2.2 ± 0.3 , and to 3.2 ± 0.4 with the increase of TEOS volume from 0.7 vol% to 1.2 vol%, and to 1.6 vol% (Figure S1B). Previous studies have reported that the nanoparticles with nanoscale surface roughness can effectively enhance the binding and adhesion of biomolecules.^{38,39} We thus selected hMSN-A16 with the greatest rambutan-like roughness as the candidate nanocarrier.

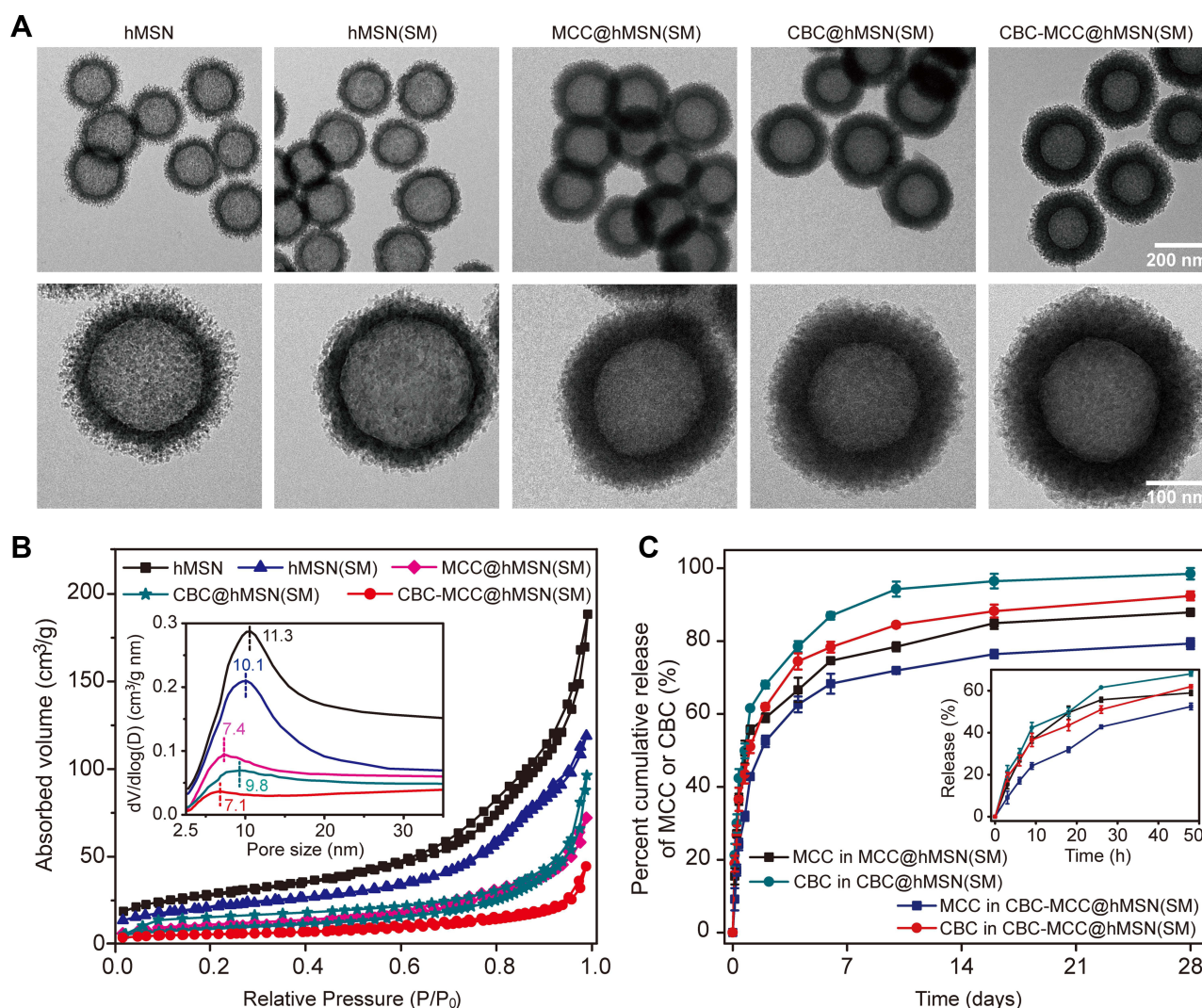


Figure 1 Characterization of CBC-MCC@hMSN(SM) complex formulation. **(A)** TEM images of hMSN, hMSN(SM), MCC@hMSN(SM), CBC@hMSN(SM), and CBC-MCC@hMSN(SM) complex formulations and their magnified TEM images. **(B)** Nitrogen adsorption-desorption isotherms of hMSN, hMSN(SM), MCC@hMSN(SM), CBC@hMSN(SM), and CBC-MCC@hMSN(SM) complex formulations. The adsorbed volume against relative pressure plot was used to calculate the specific surface area in the relative pressure (P/P_0) ranging from 0.04 to 0.1 by BET model, the pore size distribution and pore volume by BJH model, and the total pore volumes (V_t) based on the adsorbed N_2 amount at the P/P_0 of 0.995. The pore size against $dV/d\log$ plot was used to determine the effects of CBC or MCC loading on the pore size distribution. **(C)** In vitro cumulative release curves of MCC or CBC from MCC@hMSN(SM), CBC@hMSN(SM), and CBC-MCC@hMSN(SM) complex formulations. The results were shown as mean \pm SD ($n = 4$).

The nitrogen adsorption-desorption isotherms revealed that hMSNs with rough surfaces had a rather narrow average pore size, large pore volume, and high surface area. After increasing TEOS volume from 0.7 vol%, 1.2 vol% to 1.6 vol%, hMSNs had a decreased average pore size from 15.2, 13.4 to 11.3 nm (Figure S1C), increased pore volume from 0.31, 0.38 to 0.44 cm³/g, and increased specific surface area from 108.7, 126.1 to 135.0 m²/g.

The hMSNs with larger pore volumes and higher specific surface areas were suitable for filling and absorbing small molecule drugs (such as MCC) on the pore walls via relatively large mesoporous channels.^{40,41} Thus, hMSN with TEOS volume of 1.6% was selected for loading of CBC and MCC owing to the greatest surface roughness (3.2), largest pore volume (0.44 cm³/g), and highest surface area (135.0 m²/g). Although hMSN (1.6%) had the smallest average pore size (11.3 nm), it was enough to efficiently incorporate CBC, which is a kind of IgG protein with a hydrodynamic radius of <10.7 nm.⁴²

To promote the loading of MCC and CBC, we modified the surface of hMSNs with -NH₂ and PEG groups. As shown in Figure S2, the FTIR curve of hMSN(SM) had the new peaks at 1460 cm⁻¹ (bending vibration of -CH₂), 1734 cm⁻¹ (bending vibration of -C=O), and 2875 cm⁻¹ (stretching vibration of -CH₂). The hMSNs experienced a charge reversal from negative (-24.5 mV) to positive (+26.0 mV), and then to negative (-21.6 mV) due to the conversion of surface functional groups from -Si-O-H to -NH₃⁺, and then to PEG group.

After CBC and MCC were loaded into hMSN(SM), an increased average grayscale measured from the TEM images was observed (Figure 1A). The zeta potentials changed from -21.6 mV for hMSN(SM), to -2.2, -10.9 and -12.3 mV for MCC@hMSN(SM), CBC@hMSN(SM) or CBC/MCC@hMSN(SM) complex, respectively (Figure S3). As shown in Figure 1B, the surface roughness (D_p/D_a) gradually decreased from 2.5 for hMSN(SM), to 2.4 for MCC@hMSN(SM), to 2.0 for CBC@hMSN(SM) and 1.9 for CBC/MCC@hMSN(SM). Compared with hMSN(SM) nanocarrier (pore size: 11.3 nm; pore volume: 0.44 cm³/g, BET surface area: 79.1 m²/g; surface roughness: 2.5, and particle size: 257.4 nm), MCC@hMSN(SM) complex had a decreased pore size (7.4 nm), pore volume (0.12 cm³/g), and BET surface area (33.9 m²/g), a similar surface roughness (2.4), but a increased particle size (288.0 nm). When CBC was loaded into hMSN(SM), CBC@hMSN(SM) had a decreased surface roughness (2.0), pore volume (0.16 cm³/g), and BET surface area (31.4 m²/g) but an increased particle size (302.4 nm). After MCC and CBC were loaded into hMSN(SM) nanocarrier, CBC-MCC@hMSN(SM) complex had the smallest surface roughness (1.9), pore size (7.1 nm), pore volume (0.07 cm³/g), and BET surface area (18.4 m²/g), but the largest particle size (338.2 nm). The encapsulation efficiency and drug loading efficiency of CBC and MCC is shown in Table 1.

The release profiles of MCC and CBC from MCC@hMSN(SM), CBC@hMSN(SM), and CBC-MCC@hMSN(SM) complex formulations were also determined in vitro. Both MCC and CBC experienced a burst release stage (<3 h), a sustained release stage (from 3 h–24 h), and a slow release stage (24 h–28 d) from MCC@hMSN(SM), CBC@hMSN(SM), and CBC-MCC@hMSN(SM) complex. The release rate of MCC or CBC from CBC-MCC@hMSN(SM) complex was significantly lower than that of MCC or CBC from MCC@hMSN(SM) complex or CBC@hMSN(SM) complex after the burst release stage (Figure 1C).

hMSN(SM) Nanocarrier Has No Obvious Cytotoxicity and Tissue Toxicity

HRVECs and RF/6A cells were used to investigate the cytotoxicity of hMSN(SM). MTT assays showed that hMSN(SM) nanocarrier did not cause an obvious toxicity on HRVECs or RF/6A cells at the tested concentrations and the tested time points (Figure 2A–D). For tissue toxicity assays, the retinas were collected for

Table 1 Encapsulation Efficiency and Drug Loading Efficiency of MCC and CBC

| | Encapsulation Efficiency | | Drug Loading Efficiency | |
|------------------|--------------------------|-------------|-------------------------|-------------|
| | MCC | CBC | MCC | CBC |
| MCC@hMSN(SM) | 91.2 ± 2.2% | / | 22.8 ± 1.9% | / |
| CBC@hMSN(SM) | / | 82.6 ± 1.6% | / | 41.3 ± 1.2% |
| CBC-MCC@hMSN(SM) | 86.2 ± 1.6% | 78.5 ± 1.5% | 21.6 ± 1.8% | 39.3 ± 2.3% |

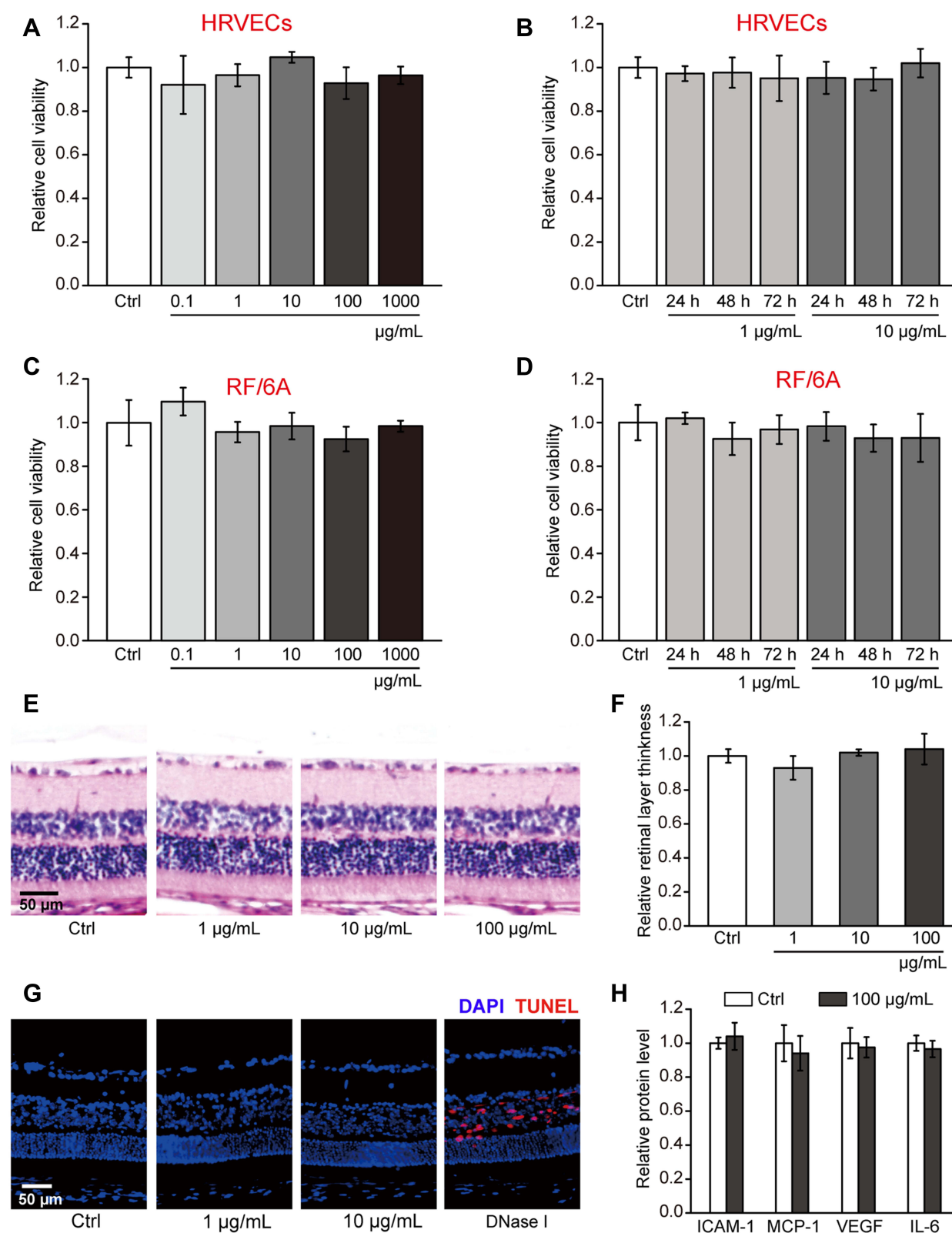


Figure 2 hMSN(SM) nanocarrier has no obvious cytotoxicity and tissue toxicity. (**A–D**) Relative cell viability of HRVECs or RF/6A cells incubated with PBS (Ctrl), or 0.1, 1, 10, 100, and 1000 µg/mL of hMSN(SM) for 24 h or incubated with 1 µg/mL and 10 µg/mL of hMSN(SM) for 24 h, 48 h, and 72 h. MTT assays were conducted to detect cell viability ($n = 4$; One-way ANOVA test). (**E** and **F**) H&E staining and quantitative analysis was conducted to detect the change of retinal thickness after intravitreal injection of 1 µg/mL, 10 µg/mL, 100 µg/mL of hMSN(SM) or left untreated (Ctrl) for 30 days ($n = 5$; Kruskal–Wallis test). (**G** and **H**) TUNEL staining and ELISA assays of the retinas of C57BL/6J mice after an intravitreal injection of 1 µg/mL, 10 µg/mL, 100 µg/mL hMSN(SM) or left untreated (Ctrl) for 30 days. TUNEL staining was conducted to detect retinal apoptosis ((**G**), $n = 5$). ELISA assays were conducted to detect the expression change of ICAM-1, MCP-1, VEGF, and IL-6 ((**H**), $n = 5$, Mann–Whitney U -test).

histopathological analysis after 30-day injection of hMSN(SM) nanocarrier. H&E staining showed that injection of hMSN(SM) nanocarrier did not disrupt the normal structures of retinal vessels (Figure 2E). The thickness of retinal layers did not show significant difference among the different groups (Figure 2F). TUNEL assays showed that injection of hMSN(SM) nanocarrier did not induce a detectable apoptosis of retinal cells (Figure 2G). ELISA assays showed that injection of hMSN(SM) nanocarrier did not alter the expression of ICAM-1, MCP-1, and IL-6 levels, suggesting that no significant inflammatory responses were observed in the retinas following the injection of hMSN(SM) nanocarrier. Moreover, the expression of VEGF level was not altered following the injection of hMSN(SM) nanocarrier (Figure 2H). Taken together, the above-mentioned results suggest that hMSN(SM) nanocarrier has no obvious cytotoxicity and tissue toxicity.

CBC-MCC@hMSN(SM) Complex Formulation Suppresses Angiogenic Effects and Inflammatory Responses in Endothelial Cells

VEGF is a critical driver of endothelial angiogenic activities during vascular dysfunction.²⁵ HRVECs were treated with VEGF to build endothelial angiogenic model in vitro. MTT assays showed that compared with Ctrl group or hMSN(SM) group, administration of MCC, MCC@hMSN(SM), CBC, CBC@hMSN(SM), or CBC-MCC@hMSN(SM) significantly decreased the viability of endothelial cells. Notably, CBC-MCC@hMSN(SM) complex had the greatest inhibitory efficiency on endothelial viability among all treated groups (Figure 3A). CBC-MCC@hMSN(SM) complex had the greater inhibitory efficiency on cell proliferation as shown by decreased Ki67 staining than hMSN(SM), MCC, MCC@hMSN(SM), CBC, or CBC@hMSN(SM), especially after 72 h culture (Figure 3B). Transwell assays and Matrigel tube formation assays showed that CBC-MCC@hMSN(SM) complex was more effective than the other 6 groups in inhibiting endothelial cell migration and tube formation (Figure 3C and D).

HRVECs were treated with LPS to build the inflammatory model in vitro. qRT-PCR and ELISA assays were conducted to detect the expression change of the angiogenic factor and inflammatory factors at the mRNA levels and protein levels. The results showed that administration of CBC@hMSN(SM) and CBC exerted an inhibitory effects on the expression of the angiogenic factor, VEGF. MCC@hMSN(SM) and MCC demonstrated an obvious inhibitory effect on the expression of the inflammatory factors, including ICAM-1, MCP-1, and IL-6 at the mRNA and protein levels (Figure 4). Notably, CBC-MCC@hMSN(SM) exhibited the greatest inhibitory effects on LPS-induced angiogenic effect and inflammatory responses as shown by the lowest expression of VEGF, ICAM-1, MCP-1, and IL-6.

CBC-MCC@hMSN(SM) Complex Formulation Suppresses CNV Formation and CNV-Related Inflammatory Responses

CBC-MCC@hMSN(SM) or an equivalent dose of free MCC or CBC were injected into the eyes of C57BL/6J mice to investigate the release profiles of MCC and CBC. In C57BL/6J mice, the amounts of MCC and CBC in the retinas at day 0 (injection date) were set as 100%. There were still about 73% of the initial CBC and 50% of the initial MCC still remained in the retinas at day 30 after the injection of CBC-MCC@hMSN(SM). By contrast, there were only 14% of the initial CBC and only 8% of the initial MCC remained in the retinas at day 30 after the injection of free CBC or MCC (Figure 5A and B).

Laser-induced CNV model was used to determine the anti-angiogenic and anti-inflammatory effects of CBC-MCC@hMSN(SM) complex. Isolectin-B4 staining showed that the administration of MCC, MCC@hMSN(SM), CBC, CBC@hMSN(SM), or CBC-MCC@hMSN(SM) could reduce the neovascular regions of RPE/choroid flat mounts at day 14 and day 21 following laser injury compared with Ctrl group or hMSN(SM)-treated group. Notably, the administration of CBC-MCC@hMSN(SM) complex had the optimal inhibitory effects on CNV formation (Figure 5C). The expression levels of ICAM-1, MCP-1, VEGF, and IL-6 were also detected in RPE/choroid flat mounts. qRT-PCR assays and ELISA assays showed that compared with Ctrl group or hMSN(SM) group, the administration of MCC, CBC, MCC@hMSN(SM), CBC@hMSN(SM), or CBC-MCC@hMSN(SM) reduced the

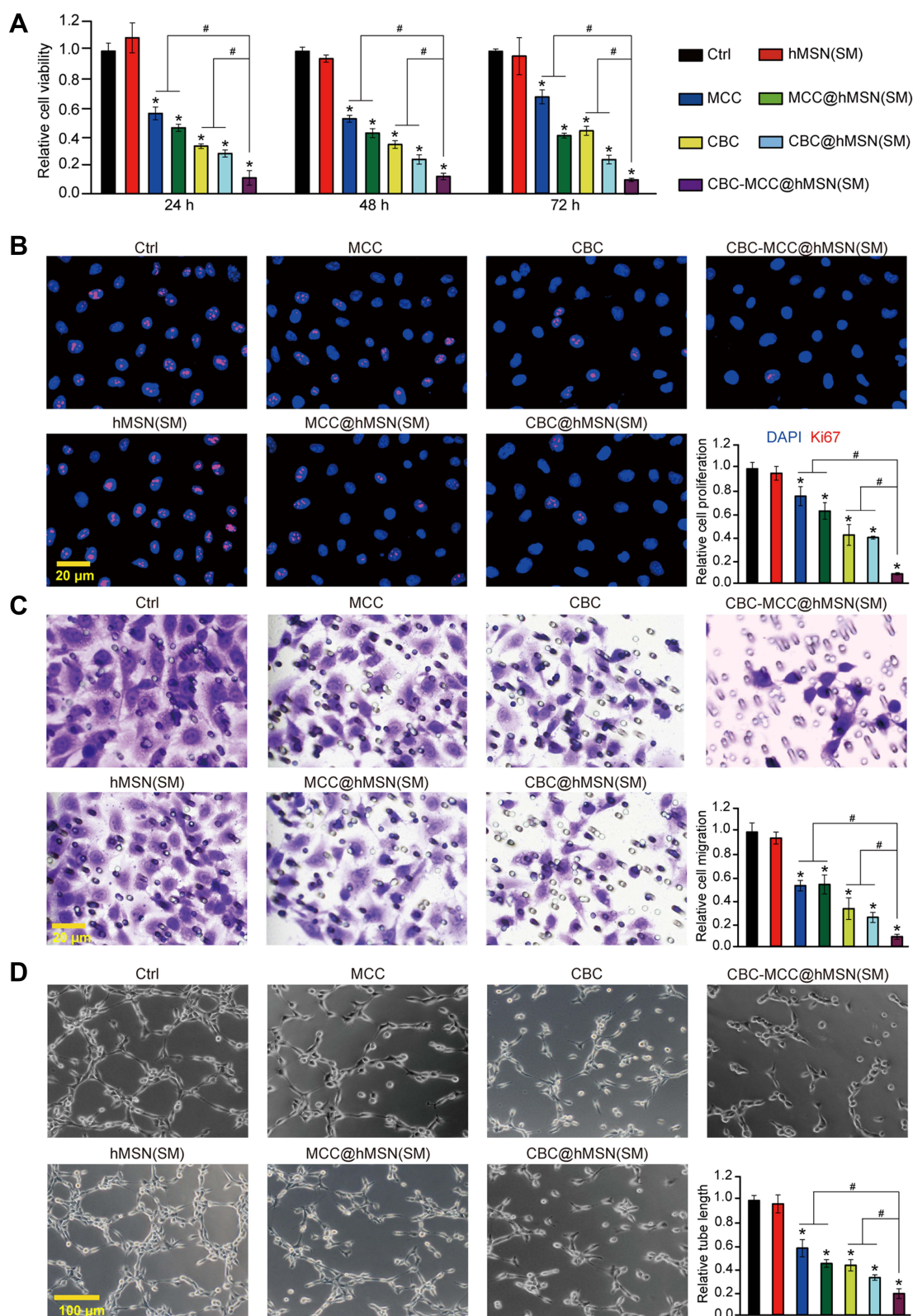


Figure 3 CBC-MCC@hMSN(SM) complex formulation suppresses angiogenic effects in endothelial cells (**A**) The viability of HRVECs incubated with VEGF (10 ng/mL) without or with hMSN(SM) (5 μ g/mL), CBC (10 μ g/mL), MCC (5 μ g/mL), CBC@hMSN(SM) (CBC: 10 μ g/mL, MCC@hMSN(SM) (MCC: 5 μ g/mL), or CBC-MCC@hMSN(SM) (CBC: 10 μ g/mL, MCC: 5 μ g/mL) for 24 h, 48 h, and 72 h. Cell viability was detected by MTT assays ($n = 4$, One-way ANOVA followed by Bonferroni test). (**B–D**) Representative images and quantitative results of cell proliferation (**B**), cell migration (**C**), and tube formation (**D**) of HRVECs treated as shown in Figure 3A for 72 h ($n = 4$, One-way ANOVA followed by Bonferroni test). VEGF-treated HRVECs were taken as the control group (Ctrl). * $P < 0.05$ vs Ctrl; # $P < 0.05$ vs CBC-MCC@hMSN(SM).

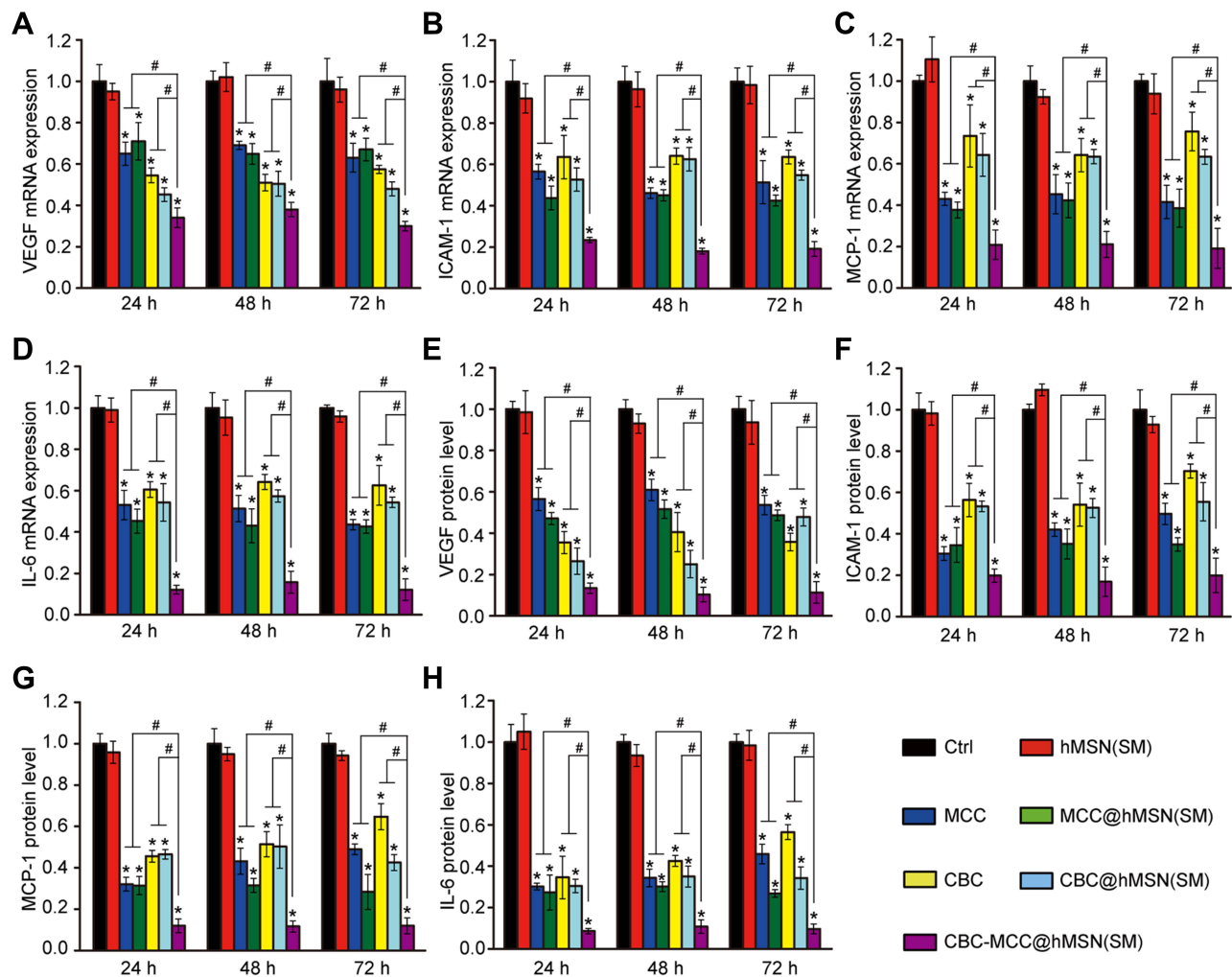


Figure 4 CBC-MCC@hMSN(SM) complex formulation suppresses LPS-induced inflammatory responses in endothelial cells. (A–H) HRVECs were cultured in the serum-starved condition for 1 h, and then incubated with LPS (100 ng/mL) without or with hMSN(SM) (5 μ g/mL), CBC solution (10 μ g/mL), MCC solution (5 μ g/mL), CBC@hMSN(SM) (CBC: 10 μ g/mL, MCC@hMSN(SM) (MCC: 5 μ g/mL), or CBC-MCC@hMSN(SM) (MCC: 5 μ g/mL, CBC: 10 μ g/mL) for 24 h, 48 h, and 72 h. qRT-PCR and ELISA assays were conducted to detect the expression of VEGF, ICAM-1, MCP-1, and IL-6 ($n = 4$, One-way ANOVA followed by Bonferroni test). * $P < 0.05$ vs Ctrl; # $P < 0.05$ vs CBC-MCC@hMSN(SM).

expression of ICAM-1, MCP-1, VEGF, and IL-6 levels in the RPE/choroid flat mounts at the mRNA and protein levels. The administration of CBC-MCC@hMSN(SM) had the greatest inhibitory effects on CNV-related inflammatory response (Figure 5D–K).

CBC-MCC@hMSN(SM) Complex Formulation Suppresses Diabetes-Induced Retinal Vascular Dysfunction and Inflammatory Responses

Diabetic retinopathy (DR) is another ocular vascular disease that causes visual impairment and blindness. Its pathogenesis is associated with retinal vascular dysfunction and inflammatory responses.³¹ Evans blue assays showed that long-term diabetes led to increased retinal vascular permeability. The administration of MCC, MCC@hMSN(SM), CBC, CBC@hMSN(SM), or CBC-MCC@hMSN(SM) could significantly alleviate diabetes-induced retinal vascular permeability. Notably, CBC-MCC@hMSN(SM) showed the best therapeutic effects on retinal vascular permeability (Figure 6A). The number of acellular capillaries was quantified to evaluate retinal vascular lesions. Trypsin digestion assays showed that long-term diabetes led to increased number of retinal acellular capillaries. The administration of MCC, MCC@hMSN(SM), CBC, CBC@hMSN(SM), or CBC-MCC@hMSN(SM) could decrease the number of retinal acellular capillaries. CBC-MCC@hMSN(SM) group had the fewest acellular capillaries among different experimental groups (Figure 6B). qRT-PCR and ELISA assays showed that

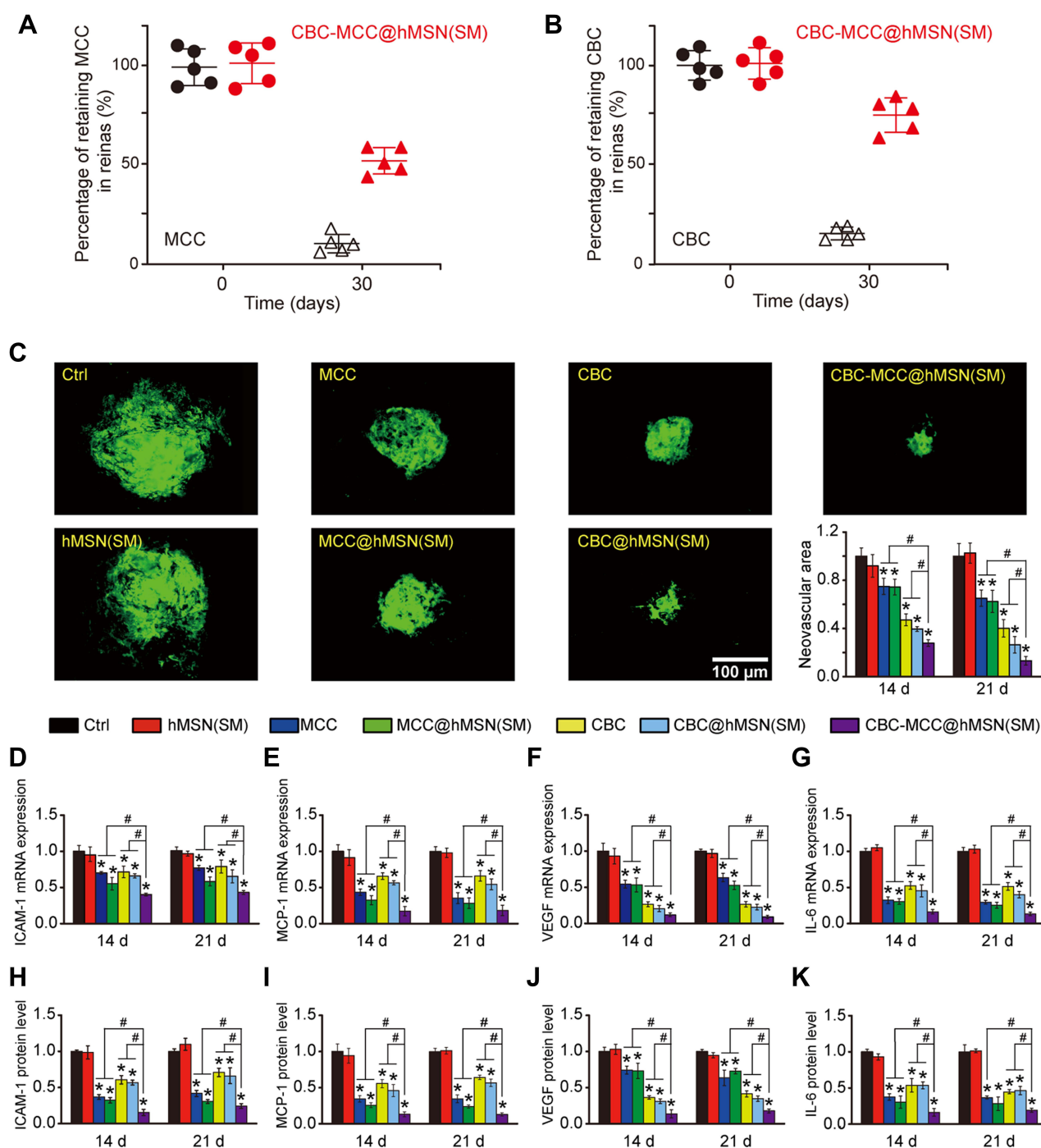


Figure 5 CBC-MCC@hMSN(SM) complex formulation suppresses CNV formation and CNV-related inflammatory responses. (**A** and **B**) Percentage of the retaining MCC (**a**) and CBC (**B**) in the retinas of C57BL/6J mice at day 0 and 30 after intravitreal injections of 1 μ L of CBC-MCC@hMSN(SM) complex (MCC: 5 mg/mL, CBC: 10 mg/mL) or an equivalent dose of MCC or CBC solution (n = 5). The amounts of MCC or CBC in the retinas at day 0 (injection date) were set as 100%. (**C**) Representative images of RPE/choroid complexes stained by Isolectin-B4 at day 21 after laser injury and the change of neovascular regions (n = 5) at day 14 and 21 after laser injury. (**D–K**) mRNA and protein expression levels of ICAM-1, MCP-1, VEGF, and IL-6 in RPE/choroid complexes detected by qRT-PCR and ELISA assays (n = 5). Kruskal–Wallis test; * $P < 0.05$ vs Ctrl; # $P < 0.05$ vs CBC-MCC@hMSN(SM).

the administration of MCC, MCC@hMSN(SM), CBC, CBC@hMSN(SM), or CBC-MCC@hMSN(SM) could reduce the expression of ICAM-1, MCP-1, VEGF, and IL-6 at the mRNA or protein levels. CBC-MCC@hMSN(SM) group showed the best inhibitory effects on diabetes-induced expression of inflammatory factors and angiogenic factor (Figure 6C–J).

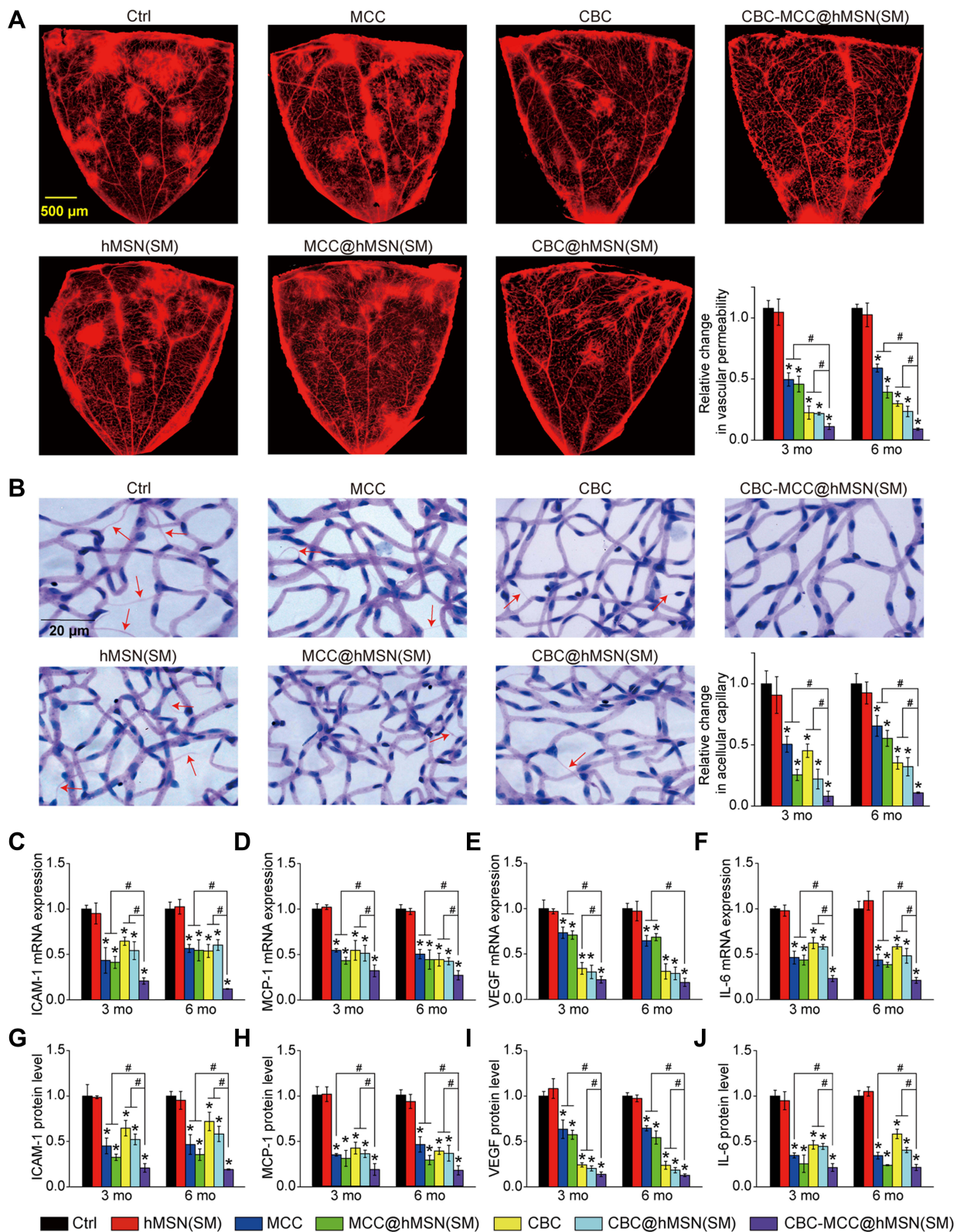


Figure 6 CBC-MCC@hMSN(SM) complex formulation suppresses diabetes-induced retinal vascular dysfunction and inflammatory responses **(A)** Representative images of flat-mounted retinas stained by Evans blue at month 6 and relative change of retinal vascular permeability at month 3 and 6 ($n = 5$) in diabetic C57BL/6 mice after intravitreal injections of 1 μ L of PBS (Ctrl), hMSN(SM) (5 mg/mL), MCC (5 mg/mL), MCC@hMSN(SM) (MCC: 5 mg/mL), CBC (10 mg/mL), CBC@hMSN(SM) (CBC: 10 mg/mL), or CBC-MCC@hMSN(SM) (MCC: 5 mg/mL, CBC: 10 mg/mL). **(B)** Retinal trypsin digestion was conducted to detect the number of acellular retinal capillaries (red arrows). Acellular capillaries were stained with PAS (Periodic Acid-Schiff)/hematoxylin and quantified in 30 random fields per retina and averaged ($n = 5$). **(C–J)** The expression levels of ICAM-1, MCP-1, VEGF, and IL-6 in the retinas were detected by qRT-PCR and ELISA assays ($n = 5$). Kruskal–Wallis test; * $P < 0.05$ vs Ctrl; # $P < 0.05$ vs CBC-MCC@hMSN(SM).

Discussion

Pathological angiogenesis and inflammatory responses are interconnected in the pathogenesis of ocular vascular diseases.⁴ Current treatments require frequent intraocular injections of anti-VEGF drugs or topical treatment with anti-inflammatory drugs.^{2,5} Herein, we provide a dual-drug nanocomposite formulation system, which could synergistically load CBC and MCC for anti-angiogenic and anti-inflammatory treatment. In this system, CBC or MCC are gradually released from CBC-MCC@hMSN(SM) complex. CBC or MCC is required to overcome the restriction of functional groups and charged groups to enter the mesoporous channels of hMSN nanocarrier. Functional groups and complicated mesoporous channels is beneficial for the sustained release of CBC or MCC from CBC-MCC@hMSN(SM) complex.

Mesoporous silica nanoparticles have emerged as the promising drug delivery systems due to the following properties, including high surface area, large pore size, good biocompatibility, and biodegradability.^{23,24} Zhang et al used the spherical mesoporous silica nanoparticles for improved oral absorption of Telmisartan (TEL). TEL loading within the pores of MSNs led to improved dissolution rate and bioavailability compared with pure drug powder.⁴³ Lu et al used a fluorescent mesoporous silica nanoparticle (FMSN) for the delivery of Camptothecin (CPT), an anti-cancer drug. Incorporation of CPT into pores of FMSNs enhanced the solubility of CPT and improved its anti-tumor efficacy.⁴⁴ Thomas et al used the magnetic actuation of mechanized nanoparticles to achieve the noninvasive remote-controlled drug release for breast cancer treatment.⁴⁵ We also used other MSN carriers to deliver nitric oxide donor or bevacizumab for the treatment of ocular diseases.^{25,26} Conbercept (CBC, 143 kDa) a big molecule drug, while MCC950 (MCC, 426 Da) is a small molecule drug. We thus required a MSN carrier for simultaneous delivery for CBC and MCC. However, the above-mentioned solid and conventional MSN types are not suitable for the co-delivery of CBC and MCC because the loading capacity and drug release dynamics are difficult to adjust in a wide range. In this study, the newly designed hMSN(SM) nanocarrier meets the requirement for the co-delivery of CBC and MCC. The rough surfaces electrostatically adsorb the big molecule drug (CBC), while the well-interconnected nanopores can encapsulate the small molecular weight drug (MCC).

The dual combination of anti-angiogenic and anti-inflammatory treatment is a promising method for treating ocular vascular disease. However, synergistic drug administration is difficult because the anti-angiogenic and anti-inflammatory drugs usually have different physical and chemical properties. Considering this problem, CBC and MCC are in sequence loaded into the hMSN(SM) system. If CBC was loaded firstly, the mesoporous channels of hMSN(SM) might be partially blocked, which could affect the load efficiency of MCC. MCC and CBC are bounded by a mass of pore channels, aminopropyl groups, and PEG chains by steric hindrance, electrostatic interaction and hydrogen bond interaction. Moreover, MCC and CBC could be continually released from CBC-MCC@hMSN(SM), which is far longer than intravitreal injection of free MCC or CBC.

When CBC and MCC is incorporated into hMSN(SM) nanocarrier, the primary concern is whether CBC-MCC@hMSN(SM) has good biocompatibility and bioactivity.²⁵ The eye is a relatively closed tissue and topical administration is often used. When CBC-MCC@hMSN(SM) is injected into the vitreous, only a small percentage of drug enters the systemic circulation. The entered drugs also experience metabolism, degradation, and absorbance by phagocytes. The remaining drug or silica nanoparticle becomes even less. Long-term silica exposure has the risk of developing serious silica-related disease, such as silicosis.^{46,47} In this study, we delivered mesoporous silica nanoparticles by intravitreal injection, which is an approach for topical medication. Silicosis is usually caused by the inhalation exposure of crystalline silica.⁴⁶ Thus, there is no need to be worried about the occurrence of silicosis caused by hMSN(SM). Previous study has reported that short-term oral administration of mesoporous silica does not induce local or systemic toxicity in mice.⁴⁸ Bioactivity assays reveal that CBC-MCC@hMSN(SM) complex is more effective than free CBC or MCC in suppressing endothelial angiogenic effects and inflammatory responses. CBC or MCC is sustainably released from CBC-MCC@hMSN(SM). The anti-angiogenic and anti-inflammatory activities of CBC-MCC@hMSN(SM) are perfectly preserved and greatly improved.

Another important concern is whether CBC-MCC@hMSN(SM) can be cleared from the eye. Previous studies have reported that MSN nanoparticles are gradually degraded into silicic acid and other soluble substances in the eye. Small molecules silicic acid and other soluble substances within eyeball could be cleared through both retinal-choroid-sclera

(RCS) pathways and anterior outflow pathways.⁴⁹ Another important evidence also suggests the bio-safety of silicon material in ophthalmology. Silicone oil has been used as the long-term tamponade agent for the treatment of retinal diseases.⁵⁰ MCC experiences the hydroxylation on the 1, 2, 3, 5, 6, 7-hexahydro-s-indacene moiety to form the major metabolite. These hydrophobic small molecules within eyeball are cleared through both retinal-choroid-sclera and anterior outflow pathways.⁵¹ The degraded components of CBC are the degraded proteins, which are predominantly cleared through the aqueous outflow pathways, including the trabecular meshwork of the chamber angle and the uveoscleral pathway.^{52,53} Thus, the biological safety of CBC-MCC@hMSN(SM) is guaranteed and trustworthy during the clinical applications.

Conclusion

In summary, the new synthesized MSN nanoparticles, hMSN(SM), have good biocompatibility and are suitable for the simultaneous delivery of a macromolecule drug (CBC) and a small molecule drug (MCC). CBC-MCC@hMSN(SM) complex nanoformulation can enhance the anti-angiogenic and anti-inflammatory efficiency in the treatment of ocular vascular diseases. Thus, this nanocomposite formulation system provides a promising strategy for the sustained suppression of ocular angiogenesis and inflammatory responses, which would improve the treatment outcomes for ocular vascular diseases. However, we did not explore the pharmacokinetic of CBC-MCC@hMSN(SM) complex in depth, which is the focus of our future research.

Acknowledgments

This research was supported by the National Natural Science Foundation of China (82171074, 81970809 and 81570859), the Scientific and Innovative Action Plan of Shanghai (19441900600), and the Natural Science Foundation of Shanghai (19ZR1408300). The sponsor or funding organization had no role in the design or conduct of this research.

Disclosure

The authors have no conflicts of interest to declare for this work.

References

- Campochiaro PA. Ocular neovascularization. *J Mol Med*. 2013;91(3):311–321. doi:10.1007/s00109-013-0993-5
- Campochiaro PA. Molecular pathogenesis of retinal and choroidal vascular diseases. *Prog Retin Eye Res*. 2015;49:67–81. doi:10.1016/j.preteyeres.2015.06.002
- Zhang SX, Ma J-X. Ocular neovascularization: implication of endogenous angiogenic inhibitors and potential therapy. *Prog Retin Eye Res*. 2007;26(1):1–37. doi:10.1016/j.preteyeres.2006.09.002
- Capitão M, Soares R. Angiogenesis and inflammation crosstalk in diabetic retinopathy. *J Cell Biochem*. 2016;117(11):2443–2453. doi:10.1002/jcb.25575
- Costa C, Incio J, Soares R. Angiogenesis and chronic inflammation: cause or consequence? *Angiogenesis*. 2007;10(3):149–166.
- Ma DHK, Chen HCJ, Lai JY, et al. Matrix revolution: molecular mechanism for inflammatory corneal neovascularization and restoration of corneal avascularity by epithelial stem cell transplantation. *Ocul Surf*. 2009;7(3):128–144.
- Stratman AN, Farrelly OM, Mikelis CM, et al. Anti-angiogenic effects of VEGF stimulation on endothelium deficient in phosphoinositide recycling. *Nat Commun*. 2020;11(1):1204.
- Wells JA, Glassman AR, Ayala AR, et al. Aflibercept, bevacizumab, or ranibizumab for diabetic macular edema. *New Engl J Med*. 2015;372(13):1193–1203.
- Sherif Z, Pleyer U. Corticosteroids in ophthalmology: past-present-future. *Ophthalmologica*. 2002;216(5):305–315.
- Pavesio CE, Decory HH. Treatment of ocular inflammatory conditions with loteprednol etabonate. *Brit J Ophthalmol*. 2008;92(4):455–459. doi:10.1136/bjo.2007.132621
- Kambhampati SP, Bhutto IA, Wu T, et al. Systemic dendrimer nanotherapies for targeted suppression of choroidal inflammation and neovascularization in age-related macular degeneration. *J Control Release*. 2021;335:527–540. doi:10.1016/j.jconrel.2021.05.035
- Luo L-J, Jian H-J, Harroun SG, Lai J-Y, Unnikrishnan B, Huang -C-C. Targeting nanocomposites with anti-oxidative/inflammatory/angiogenic activities for synergistically alleviating macular degeneration. *Appl Mater Today*. 2021;24:101156. doi:10.1016/j.apmt.2021.101156
- Liu K, Song YP, Xu GZ, et al. Conbercept for treatment of neovascular age-related macular degeneration: results of the randomized Phase 3 Phoenix study. *Am J Ophthalmol*. 2019;197:156–167. doi:10.1016/j.ajo.2018.08.026
- Zhou PX, Zheng SQ, Wang ET, Men P, Zhai SD. Conbercept for treatment of neovascular age-related macular degeneration and visual impairment due to diabetic macular edema or pathologic myopia choroidal neovascularization: a systematic review and meta-analysis. *Front Pharmacol*. 2021;12:696201. doi:10.3389/fphar.2021.696201
- Jin E, Yin H, Li X, Zhao M. Short-term outcomes after intravitreal injections of conbercept versus ranibizumab for the treatment of retinopathy of prematurity. *Retina*. 2018;38(8):1595–1604. doi:10.1097/IAE.0000000000001763

16. Coll RC, Hill JR, Day CJ. MCC950 directly targets the NLRP3 ATP-hydrolysis motif for inflammasome inhibition. *Nat Chem Biol.* 2019;15(6):556–559. doi:10.1038/s41589-019-0277-7
17. Corcoran SE, Halai R, Cooper MA, Page C. Pharmacological inhibition of the nod-like receptor family pyrin domain containing 3 inflammasome with MCC950. *Pharmacol Rev.* 2021;73(3):968–1000. doi:10.1124/pharmrev.120.000171
18. Weng YH, Liu J, Jin SB, Guo WS, Liang XJ, Hua ZB. Nanotechnology-based strategies for treatment of ocular disease. *Acta Pharm Sin B.* 2017;7(3):281–291. doi:10.1016/j.apsb.2016.09.001
19. Nguyen DD, Lai J-Y. Synthesis, bioactive properties, and biomedical applications of intrinsically therapeutic nanoparticles for disease treatment. *Chem Eng J.* 2022;435:134970. doi:10.1016/j.cej.2022.134970
20. Kankala RK, Han Y-H, Na J, et al. Nanoarchitected structure and surface biofunctionality of mesoporous silica nanoparticles. *Adv Mater.* 2020;32(23):e1907035. doi:10.1002/adma.201907035
21. Yang WJ, Yu YR, Shou X, Zhang DG, Liang GF, Zhao YJ. Hedgehog-inspired magnetic nanoparticles for effectively capturing and detecting exosomes. *NPG Asia Mater.* 2021;13(1):78. doi:10.1038/s41427-021-00346-4
22. Pan PP, Yue Q, Li J, et al. Smart cargo delivery system based on mesoporous nanoparticles for bone disease diagnosis and treatment. *Adv Sci.* 2021;8(12):2004586. doi:10.1002/adv.202004586
23. Shen DK, Yang JP, Li XM, et al. Biphasic stratification approach to three-dimensional dendritic biodegradable mesoporous silica nanospheres. *Nano Lett.* 2014;14(2):923–932. doi:10.1021/nl404316v
24. Tang F, Li L, Chen D. Mesoporous silica nanoparticles: synthesis, biocompatibility and drug delivery. *Adv Mater.* 2012;24(12):1504–1534. doi:10.1002/adma.201104763
25. Sun J-G, Jiang Q, Zhang X-P, et al. Mesoporous silica nanoparticles as a delivery system for improving antiangiogenic therapy. *Int J Nanomed.* 2019;14:1489–1501. doi:10.2147/IJN.S195504
26. Hu CC, Sun JG, Zhang Y, et al. Local delivery and sustained-release of nitric oxide donor loaded in mesoporous silica particles for efficient treatment of primary open-angle glaucoma. *Adv Healthc Mater.* 2018;7(23):e1801047. doi:10.1002/adhm.201801047
27. Liao Y-T, Lee C-H, Chen S-T, Lai J-Y, Wu KC-W. Gelatin-functionalized mesoporous silica nanoparticles with sustained release properties for intracameral pharmacotherapy of glaucoma. *J Mater Chem B.* 2017;5(34):7008–7013. doi:10.1039/C7TB01217A
28. Song H, Ahmad Nor Y, Yu MH, et al. Silica nanopollens enhance adhesion for long-term bacterial inhibition. *J Am Chem Soc.* 2016;138(20):6455–6462. doi:10.1021/jacs.6b00243
29. Lyu N, Zhao YJ, Xiang J, et al. Inhibiting corneal neovascularization by sustainably releasing anti-VEGF and anti-inflammation drugs from silica-thermogel nanohybrids. *Mater Sci Eng C.* 2021;128:112274. doi:10.1016/j.msec.2021.112274
30. Chung T-W, Liu D-Z, Wang S-Y, Wang S-S. Enhancement of the growth of human endothelial cells by surface roughness at nanometer scale. *Biomaterials.* 2003;24(25):4655–4661. doi:10.1016/S0142-9612(03)00361-2
31. Shan K, Liu C, Liu B-H, et al. Circular noncoding RNA HIPK3 mediates retinal vascular dysfunction in diabetes mellitus. *Circulation.* 2017;136(17):1629–1642. doi:10.1161/CIRCULATIONAHA.117.029004
32. Alnuqaydan AM, Almutary A, Bhat GR, et al. Evaluation of the cytotoxic, anti-inflammatory, and immunomodulatory effects of Withaferin A (WA) against lipopolysaccharide (LPS)-induced inflammation in immune cells derived from BALB/c mice. *Pharmaceutics.* 2022;14(6):1256. doi:10.3390/pharmaceutics14061256
33. Guo ZH, Shi LQ, Feng HY, et al. Reduction-sensitive nanomicelles: delivery celastrol for retinoblastoma cells effective apoptosis. *Chin Chem Lett.* 2021;32(3):1046–1050. doi:10.1016/j.ccl.2020.03.066
34. Di Y, Xu HY, Ye JJ, Guo ZJ. A study on the drug concentration in fellow eyes after unilateral intravitreal injection of conbercept into New Zealand rabbit eyes. *Front Pharmacol.* 2021;12:783057. doi:10.3389/fphar.2021.783057
35. Biemmi V, Milano G, Ciullo A, et al. Inflammatory extracellular vesicles prompt heart dysfunction via TLR4-dependent NF- κ B activation. *Theranostics.* 2020;10(6):2773–2790. doi:10.7150/thno.39072
36. Lambert V, Lecomte J, Hansen S, et al. Laser-induced choroidal neovascularization model to study age-related macular degeneration in mice. *Nat Protoc.* 2013;8(11):2197–2211. doi:10.1038/nprot.2013.135
37. Liu C, Ge H-M, Liu B-H, et al. Targeting pericyte-endothelial cell crosstalk by circular RNA-cPWWP2A inhibition aggravates diabetes-induced microvascular dysfunction. *Proc Natl Acad Sci.* 2019;116(15):7455–7464. doi:10.1073/pnas.1814874116
38. Song H, Yu MH, Lu Y, et al. Plasmid DNA delivery: nanotopography matters. *J Am Chem Soc.* 2017;139(50):18247–18254. doi:10.1021/jacs.7b08974
39. Niu YT, Yu MH, Hartono SB, et al. Nanoparticles mimicking viral surface topography for enhanced cellular delivery. *Adv Mater.* 2013;25(43):6233–6237. doi:10.1002/adma.201302737
40. Gou KJ, Wang YM, Xie LL, et al. Synthesis, structural properties, biosafety and applications of chiral mesoporous silica nanostructures. *Chem Eng J.* 2021;421(2):127862.
41. Nakki S, Rytönen J, Nissinen T, et al. Improved stability and biocompatibility of nanostructured silicon drug carrier for intravenous administration. *Acta Biomater.* 2015;13:207–215.
42. Heidebrecht HJ, Kulozik U. Fractionation of casein micelles and minor proteins by microfiltration in diafiltration mode. Study of the transmission and yield of the immunoglobulins IgG, IgA and IgM. *Int Dairy J.* 2019;93:1–10.
43. Zhang Y, Zhi Z, Jiang T, Zhang J, Wang Z, Wang S. Spherical mesoporous silica nanoparticles for loading and release of the poorly water-soluble drug telmisartan. *J Control Release.* 2010;145(3):257–263.
44. Lu J, Liang M, Zink JI, Tamanoi F. Mesoporous silica nanoparticles as a delivery system for hydrophobic anticancer drugs. *Small.* 2007;3(8):1341–1346.
45. Thomas CR, Ferris DP, Lee JH, et al. Noninvasive remote-controlled release of drug molecules in vitro using magnetic actuation of mechanized nanoparticles. *J Am Chem Soc.* 2010;132(31):10623–10625.
46. Leung CC, Yu IT, Chen W. Silicosis. *Lancet.* 2012;379(9830):2008–2018.
47. Su C, Liu Y, Li R, Wu W, Fawcett JP, Gu J. Absorption, distribution, metabolism and excretion of the biomaterials used in Nanocarrier drug delivery systems. *Adv Drug Deliv Rev.* 2019;143:97–114.
48. Cabellos J, Gimeno-Benito I, Catalán J, et al. Short-term oral administration of non-porous and mesoporous silica did not induce local or systemic toxicity in mice. *Nanotoxicology.* 2020;14(10):1324–1341.

49. Choi E, Kim S. Surface pH buffering to promote degradation of mesoporous silica nanoparticles under a physiological condition. *J Colloid Interface Sci.* **2019**;533:463–470.
50. Chen Y, Kearns VR, Zhou L, et al. Silicone oil in vitreoretinal surgery: indications, complications, new developments and alternative long-term tamponade agents. *Acta Ophthalmol.* **2021**;99(3):240–250.
51. Salla M, Butler MS, Pelingon R, et al. Identification, synthesis, and biological evaluation of the major human metabolite of NLRP3 inflammasome inhibitor MCC950. *ACS Med Chem Lett.* **2016**;7(12):1034–1038.
52. El Sanharawi M, Kowalczuk L, Touchard E, Omri S, de Kozak Y, Behar-Cohen F. Protein delivery for retinal diseases: from basic considerations to clinical applications. *Prog Retin Eye Res.* **2010**;29(6):443–465.
53. Mandal A, Pal D, Agrahari V, Trinh HM, Joseph M, Mitra AK. Ocular delivery of proteins and peptides: challenges and novel formulation approaches. *Adv Drug Deliv Rev.* **2018**;126:67–95.

International Journal of Nanomedicine

Dovepress

Publish your work in this journal

The International Journal of Nanomedicine is an international, peer-reviewed journal focusing on the application of nanotechnology in diagnostics, therapeutics, and drug delivery systems throughout the biomedical field. This journal is indexed on PubMed Central, MedLine, CAS, SciSearch®, Current Contents®/Clinical Medicine, Journal Citation Reports/Science Edition, EMBase, Scopus and the Elsevier Bibliographic databases. The manuscript management system is completely online and includes a very quick and fair peer-review system, which is all easy to use. Visit <http://www.dovepress.com/testimonials.php> to read real quotes from published authors.

Submit your manuscript here: <https://www.dovepress.com/international-journal-of-nanomedicine-journal>